Green Chemistry

Accepted Manuscript

ROYAL SOCIETY OF CHEMISTRY

www.rsc.org/greenchem

TOC Graphics

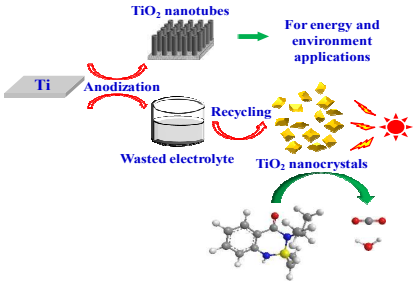

To prepare TiO_2 single crystals by recycling wasted ethylene glycol electrolyte from the widely-used anodic process for efficient photocatalytic water treatment.

Cite this: DOI: 10.1039/c0xx00000x

www.rsc.org/xxxxxx

Paper

Chemical recycling of the wasted anodic electrolyte from TiO_2 nanotube preparation process to synthesize facet-controlled TiO_2 single crystals as an efficient photocatalyst

Ai-Yong Zhang, Lu-Lu Long, Chang Liu, Wen-Wei Li and Han-Qing Yu*

Received (in XXX, XXX) Xth XXXXXXXXX 20XX, Accepted Xth XXXXXXXXX 20XX
DOI: 10.1039/b000000x

Anodization has been reported an effective electrochemical method to prepare vertically ordered, upright oriented TiO_2 nanotubes for efficient photocatalysis, solar cells and many other fields. However, this process generates a large amount of residual anodic electrolytes that are rich in toxic fluorides, which are usually wasted and cause environmental contamination. Here, we proposed a facile and effective method to prepare both pristine and N-doped TiO_2 nanocrystals based on the recycling of wasted ethylene glycol electrolyte from widely-used anodic process. Under identical conditions, both the pristine and N-doped TiO_2 nanocrystals exhibited a nearly twice higher photocatalytic activity in decomposition of humic acids and bentazone than Degussa P25, one of the best commercial TiO_2 photocatalysts. The preparation method held obvious economic and environmental benefits. The prepared TiO_2 nanocrystals possessed superior photocatalytic degradation capacities for refractory pollutants, and could be used for efficient water treatment.

1. Introduction

Anodization has been reported an effective and facile electrochemical method to prepare one-dimensional TiO_2 nanotubes (TNTs) for efficient photocatalysis, solar cells, electrochromic devices and many other fields.[1] The as-prepared highly ordered, upright oriented TNTs are anticipated to possess a high surface-to-volume ratio and provides a convenient way for photogenerated electrons to be transferred. Therefore, the faster transport, slower recombination and the resultant higher charge-collection efficiency of highly oxidative photocarriers can be anticipated, all of which will dramatically improve catalytic performance.[2] However, this synthesis process generates a large amount of residual anodic electrolytes that are rich in toxic fluorides due to the interactions among the three simultaneous processes. Currently, the typical composition of wasted anodic electrolyte from TNTs preparation is the newly-formed $[TiF_6]^{2-}$ complexes, resulting from the chemical dissolution of TiO_2 by F^- highly dispersed in either aqueous or non-aqueous supporting electrolyte. The latter includes a variety of polar organic solvents, such as ethylene glycol (EG), glycerol, dimethyl sulfoxide, formamide and N-methylformamide, in combination with HF, KF, NaF, NH_4F, Bu_4NF or $BnMe_3NF$[1] These residual anodic electrolytes are usually wasted and cause environmental contamination. From this point, it is apparent that significant economic and environmental benefits can be achieved if we could chemically recycle these wasted anodic electrolytes.

In recent years, TiO_2 photocatalytic process has shown a great potential as a low-cost, environmental friendly and sustainable treatment technology to align with the "zero" waste scheme in water/wastewater industries.[3] However, invalid recombination of active photocarriers can readily occur in the bulk and on the surface of TiO_2 accompanied with heat releasing,[4,5] which leads to high energy consumption and low degradation efficiency of organic pollutants. Therefore, how to substantially enhance the separation and transfer of photocarriers as well as their effectiveness is of high importance for photocatalytic water treatment.

It is well documented that TiO_2 surface and catalytic properties are closely associated with its crystal structures and exposed facets.[6-8] Single-crystal anatase TiO_2 has been widely used for various photocatalytic reactions. Compared with polycrystalline TiO_2, the single crystals with a high crystalline usually possess a much higher electronic conductivity and lower electron transfer resistance because of their continuous and ordered interior crystal structure, which favors the separation and transfer of photocarriers and organics decomposition. However, most available TiO_2 crystals are dominated by the thermodynamically stable {101} facets with a low surface free energy (0.44 J/m^2). Compared to the low-energy {101} facets, the arrangement and category of constituent atoms on high-energy {001} facets (0.90 J/m^2) govern its unique geometrical and electronic structures, and its surface functional groups considerably affect its stability, adsorptive property and catalytic activity. All these features make crystals with {001} facets highly efficient for photocatalytic contaminant degradation.[9-11] Thus, the tailored synthesis of TiO_2 crystals with exposed {001} facets is highly desirable for photocatalytic water treatment.

Up to now, tailored synthesis of anatase TiO_2 single crystals have been reported, but mainly completed in aqueous or organic liquid phases that contain specific capping agents (typically, fluoride). The exposed high-energy {001} facets are thermodynamically stabilized by the selectively reduced surface energy via anisotropic surface modification, and thus the final truncated octahedral crystal shape is effectively controlled.[8] This is because the reaction dynamics and the nucleation process can be readily controlled by selecting suitable titania precursors, changing the reaction medium (solvents) or the capping agents, and controlling the reaction temperature and pressure.[12-18] However, a relatively long period and high pressure are usually needed in these preparation methods.

Another barrier of TiO_2 single crystals for photocatalytic water treatment is their limited solar energy utilization capacity, which can substantially raise the running cost in practical applications. Although the spectral response of polycrystalline TiO_2 can be extended to visible light range by doping with nonmetal elements, especially N,[19] it is difficult to incorporate dopants into the well-faceted TiO_2 single crystals due to their high crystallinity.[20] Moreover, the dose of dopant precursors would inevitably influence the nucleation and growth of TiO_2 crystals.[21-26] Recently, to make {001}-exposed TiO_2 single crystals visible-light responsive, titania precursors such as TiN, TiS_2 and TiC are used to incorporate nonmetal dopants (such as N, S, C, etc.) into bulk crystals.[8,20,21] In addition to this one-pot strategy, a two-pot approach is also applied to prepare N-doped, N, S-codoped, N, F-codoped and Er-doped TiO_2 crystals.[22-26] The pristine or single-doped TiO_2 crystals are firstly prepared by either hydrothermal or solvothermal system, then calcinated in NH_3 or air at 400-500°C for 2-3 h to incorporate anionic or cationic dopants into bulk crystals. Obviously, the facile one-pot doping strategy is highly precursor-dependent, while the combined two-pot doping strategy is complicated and time-consuming. Therefore, how to facilely and effectively prepare TiO_2 crystals with visible-light photoactivity is another big challenge for pollutant degradation.

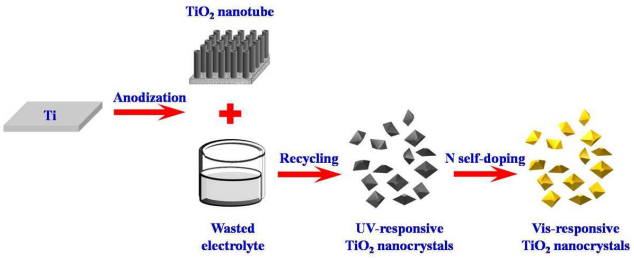

Scheme 1 Representative illustration of TiO_2 nanocrystals synthesized via calcination of wasted anodic electrolyte from anodic oxidation.

Herein, anatase TiO_2 nanocrystals with exposed {001} facets were effectively prepared for pollutant degradation by recycling the wasted anodic electrolyte containing EG, the most typical organic solvent for anodic TNTs (Scheme 1). With this method, the as-prepared TiO_2 nanocrystals could even be self-doped by N atom to gain visible-light photoactivity for water treatment. To evaluate the effectiveness of the prepared TiO_2 nanocrystals and the feasibility of applying them for water treatment, humic acids (HAs), the main natural organic matters in water, and bentazone, a typical and widely used herbicide, were selected as the target pollutant for the phtocatalytic degradation tests. In addition, Degussa P25 benchmark, one of the best commercial TiO_2,[27-29] was also tested in parallel for comparison.

2. Experimental

2.1 Preparation of pristine and N-doped TiO_2 single crystals

The wasted milk-like electrolyte (Fig. S1) was collected from the anodic process and calcinated in muffle furnace at 300-800°C for 1-10 h under air atmosphere (at a ramping rate of 1-20°C/min). This electrolyte was comprised of the newly-formed $(NH_4)_2TiF_6$ from the chemical dissolution of TiO_2 by F^- in the presence of residual EG, H_2O and NH_4F (Figs. 1, S2 and S3). By altering the calcination conditions, the color and size of the particles, the percentage of exposed {001} facets and the responsive spectrum could be adjusted in a wide range after being cooled to room temperature. Then, the samples were thoroughly rinsed with distilled water until pH exceeded 7.0. Finally, the collected precipitates were dried in a vacuum oven at 60°C for 5 h.

2.2 Characterization

The morphology and structure of the TiO_2 crystals were characterized by field-emission scanning electron microscope (FE-SEM, SIRION200, FEI Co., the Netherlands), high-resolution transmission electron microscope and selected-area electron diffraction (HRTEM/SAED, JEM-2100, JEOL Co., Japan) and scanning transmission electron microscope (STEM, JEM-ARM200F, JEOL Co., Japan). The surface area was measured by using the Brunauer-Emmett-Teller method with a Builder 4200 instrument (Tristar II 3020M, Micromeritics Co., USA) at liquid nitrogen temperature. X-ray diffraction (XRD, X'Pert, PANalytical BV, the Netherlands) was used to analyze the crystal structure. The diffuse reflectance spectra (DRS) were measured using a UV/Vis spectrophotometer (UV 2550, Shimadzu Co., Japan). The chemical compositions and valence band spectra were characterized by energy dispersive X-ray analyzer (EDX, GENESIS, EDAX Co., USA) fitted to the SEM chamber and X-ray photoelectron spectroscopy (XPS, PHI 5600, Perkin-Elmer Inc., USA), respectively. The Mott-Schottky plots were measured using a three-electrode system in 0.1 M Na_2SO_4 aqueous solution by impedance measurement at the fixed frequency of 1000 Hz between the applied voltage range of 0-1 V. Steady and time-resolved fluorescence emission spectra were recorded at room temperature with a fluorescence spectrophotometer (FLSP-920, Edinburgh Instruments Co., UK). The thermal property was determined by thermal gravimetric analysis (TGA, SDTA 851e, Mettler-Toledo, Switzerland) from 20 °C to 800 °C at a rate of 20 °C min^{-1} under air atmosphere.

The photocatalytic properties of TiO_2 nanocrystals were evaluated by short-circuit photocurrent in a conventional three-electrode system, and amount of generated ·OH under UV irradiation (200-400 nm). The tests were conducted in a home-made photoreactor with an effective volume of 60 ml. The light source was a 500 W Xe arc lamp (PLS-SXE500, Beijing Trusttech Co., China), with a 10 cm infrared water filter and a Pyrex filter (λ > 200 nm). For each test, 50 ml solution was used. Fluorescence spectra were regularly recorded using a

spectrofluorophotometer (RF-5301PC, Shimadzu Co., Japan).

2.3 HAs and bentazone degradation tests

The photocatalytic activities of the prepared TiO_2 crystals were evaluated in terms of the decomposition of HAs (1.98 and 10.75 mg/L in total organic carbon, TOC) and bentazone (3.0 mg/L) under UV (200-420 nm) or visible light (420-770 nm) irradiation. The tests were conducted in a 60-ml photoreactor at ambient temperature. The light source was a 500 W Xe arc lamp (PLS-SXE500, Trusttech Co., China). Light passed through a 10 cm infrared water filter and a UV cut-off filter ($\lambda > 420$ nm) for the visible light irradiation or a Pyrex filter ($\lambda > 200$ nm) for UV light irradiation. For each test, 50 ml of HAs or bentazone solution and 1000 mg/L of TiO_2 slurry were used. To make the fluorinated surface clean and fluorine-free, the as-prepared TiO_2 and $TiO_{2-x}N_x$ crystals were repeatedly washed to remove the fluoride ions using 1.0 M NaOH aqueous solution before each usage. The commercial Degussa P25 benchmark has a mean particle size of about 25 nm, anatase/rutile = 80:20, BET surface area of about 50 m^2/g (Degussa Co, Germany).

The UV-visible absorption and fluorescence spectra of the irradiated filtrate solutions were recorded using a UV-visible spectrophotometer (UV-2401PC, Shimadzu Co., Japan) and a spectrofluorophotometer (RF-5301PC, Shimadzu Co., Japan) respectively. The bentazone concentration was determined using high-performance liquid chromatography (HPLC-1100, Agilent Inc., USA) with a Hypersil-ODS reversed-phase column and detected at 254 nm using a VWD detector. The mobile phase was a mixture of water and methanol (40:60) delivered at a flow rate of 1 mL/min. Mineralization efficiency was estimated from the TOC removal (Vario, Elementar Co., Germany).

3. Results and discussion

3.1 Chemical composition of the wasted ethylene glycol anodic electrolyte

Although it is theoretically well documented that the $[TiF_6]^{2-}$ complex could be formed from the chemical dissolution of TiO_2 in the presence of F^- in the supporting electrolyte.[1] However, no detailed experimental proof is available in literature. To take insight into the chemical compositions of the wasted anodic electrolyte and provide sufficient information about the precursor for the subsequent TiO_2 nanocrystals preparation, more experimental analysis was consequently needed. In this study, the produced milk-like wasted anodic electrolyte from TNTs preparation was first filtered by 0.45 μm microfiltration membrane to remove most of EG, H_2O and NH_4F, and a transparent sol film was obtained; then this sol film was washed with alcohol solvent several times to completely remove the residual EG in sol, and a white powder film was obtained; after drying in vacuum for 60 min, 0.41 g of white powder was obtained (Fig. 1).

To determine the chemical composition of this white powder, XPS measurement was carried out, and the results show that the chemical composition and characteristic binding energies were intrinsically identical to those of the standard $(NH_4)_2TiF_6$ sample (99.99% trace metals basis, Sigma-Aldrich, USA) (Fig. 1A and S2). Moreover, thermogravimetry-differential thermal analysis (TG-DTA) analysis further confirmed the change behavior of its crystal structures. It was found that there were three apparently endothermic peaks at 283ºC ($(NH_4)_2TiF_6 \rightarrow NH_4TiOF_3$), 343ºC ($NH_4TiOF_3 \rightarrow TiOF_2$) and 411ºC ($TiOF_2 \rightarrow TiO_2$), respectively. When the temperature exceeded 480ºC, the residual weight changed slightly, indicating that TiO_2 became the main component in the product. The crystal structure change behaviors were intrinsically identical to those of the reference $(NH_4)_2TiF_6$ sample (Fig. 1B and S3), and agreed with the XPS measurements. However, it should be mentioned that some TG deviations from that of the pure reference were observed, which might be mainly ascribed to the relatively complicated chemical composition of the extract from the wasted anodic electrolyte.

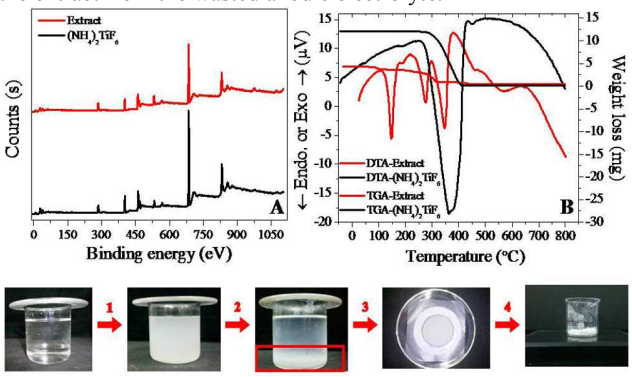

Fig. 1 Extraction and analysis of the produced wasted anodic electrolyte from anodization process. 1: anodic oxidation, 2: gravitational precipitation, 3: micro-membrane filtration, 4: ethanol rinsing and vacuum drying, A: XPS, B: TG analysis.

Therefore, the chemical compositions of anodic wasted electrolyte for TiO_2 nanocrystals preparation should mainly be the newly-formed $(NH_4)_2TiF_6$ from the chemical dissolution of TiO_2 by F^- as well as some residual EG, H_2O and NH_4F, no other main contaminants were intentionally introduced. However, in the calcination process to form TiO_2 nanocrystals, the real effective components of wasted anodic electrolyte should be $(NH_4)_2TiF_6$ and EG, because H_2O and NH_4F could quickly be evaporated or decomposed due to their little contents and the increased calcinations temperature. The residual EG might be a synergistic capping agent and reaction medium, both of which are of high importance for the formation of TiO_2 nanocrystals with exposed high-energy {001} facets.

3.2 TiO_2 nanocrystals derived from the wasted ethylene glycol anodic electrolyte

In a typical procedure, 20 ml of concentrated wasted anodic electrolyte after ultrasonic treatment was calcinated at 500°C or 600°C for 3 h with a ramping rate of 3 °C/min, and approximately 0.5 g of yellow or white powders could be produced after being cooled to room temperature. Fig. 2A shows the SEM image of TiO_2 particles prepared at 600°C for 3 h with a ramping rate of 5 °C/min. The obtained white powders (inset of Fig. 2A) were comprised of well-defined decahedral particles with a rectangular outline, i.e., truncated bipyramids, while the yellow $TiO_{2-x}N_x$ particles prepared at 500°C (Fig. 2B) under similar conditions were also comprised of well-defined

decahedral particles with a rectangular outline (Fig. 2C). In this approach, the sintering temperature, duration ramping rate, and the $[TiF_6]^{2-}$ concentration in the residual electrolyte played important roles in the formation of TiO_2 NCs and their self-doping (Figs. S4-7). Compared to the pristine TiO_2 crystals, the N self-doping with a ca. at.% of 0.62 caused no significant change in morphological characteristics. The origin of this doped N was from the used NH_4F in the anodic electrolyte, which was the only N-containing reagent and could be efficiently decomposed in the synthesis process. Thus, the N self-doping of TiO_2 crystals might be achieved by thermal nitriding using the newly-generated NH_3 from NH_4F decomposition. Moreover, both the pristine and N-doped samples had a size range of 100-300 nm and a high specific surface area of ca. 11.0 $m^2 g^{-1}$ (Fig. S8), which was much larger than that of the micro-sized decahedral particles.[13] Usually, TiO_2 crystals are randomly aggregated into micro-sized truncated octahedral bipyramids with a low surface area, and the nano-sized bipyramids are seldom obtained.[14]

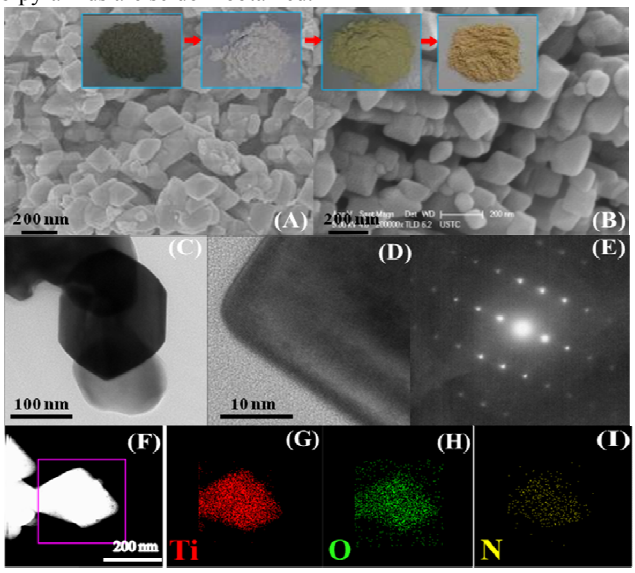

Fig. 2 SEM, HRTEM and STEM images and SAED pattern of TiO_2 (A, C, D and E) and $TiO_{2-x}N_x$ (B, F, G, H and I) prepared by calcinating wasted anodic electrolyte in air atmosphere at 600 and 500°C, respectively.

Fig. 2D and E shows the HRTEM images and the SAED pattern (indexed as the [001] zone axis diffraction) of a truncated decahedral bipyramids. The top and bottom facets of the nanosheets were the (001) planes, and the lattice spacing parallel to the top and bottom facets was ca. 0.235 nm, corresponding to the (001) planes of the anatase TiO_2 nanocrystal with clear crystalline lattice fringes. In addition, uniform lattice fringes were clearly observed across the images, confirming a well-oriented aggregation of TiO_2 nanocrystals. Moreover, to further investigate the distribution of N in the doped TiO_2 nanocrystals, STEM elemental mapping was also performed. The corresponding elemental maps demonstrate the uniform distribution of N over the entire volume of the sphere (Fig. 2F-I).

Fig. 3A shows the nitrogen adsorption-desorption isotherms and pore-size distribution curves (inset) of the TiO_2 and $TiO_{2-x}N_x$ samples. The BET surface areas, pore volumes and average pore sizes were measured to be 11.75 and 10.23 $m^2 g^{-1}$, 0.09 and 0.085 cm^3/g, and 43.4 and 38.0 nm, respectively. The loop ring of $TiO_{2-x}N_x$ almost overlapped with that of TiO_2, without any obvious change of pore size distribution. This clearly suggests that N self-doping did not destroy the porous structure of the pristine TiO_2 nanocrystals. The nanopores (or the generation of hysteresis loops) came from the aggregation of nanocrystals due to the absence of mesopores and macropores in a single nanocrystal. Such organized porous structure is crucial for the photocatalytic applications because it enables efficient transport of both reactant molecules and products. In addition, the measured average pore sizes were much less than the average side lengths. This is attributed to the fact that these nanocrystals were not individually dispersed. Instead, they were easily connected with each other along [001] direction to minimize the surface energy, which finally led to the formation of mesopores.

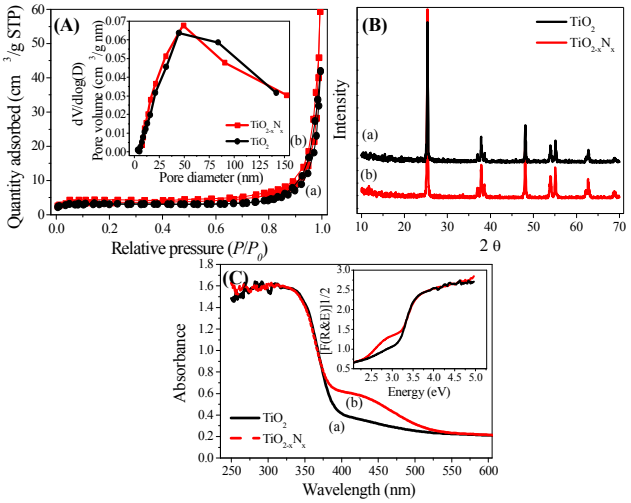

Fig. 3 Nitrogen sorption-desorption isotherms (A), XRD patterns (B) and DRS spectra (C) of the TiO_2 (a) and $TiO_{2-x}N_x$ (b).

Fig. 3B shows the XRD patterns of the calcinated TiO_2 and $TiO_{2-x}N_x$ nanocrystals. The diffraction peaks matched those of anatase TiO_2 (JCPDS No. 21-1272) well, and the obvious broadening of the diffraction peaks might be attributed to the relatively small crystallize sizes of the two prepared samples. Moreover, the intensities of (004) diffractions were observed to be broader than those of (101) diffractions, indicating an oriented crystal growth of the two nanocrystals along special axis.

The absorption properties of the TiO_2 and $TiO_{2-x}N_x$ were examined using DRS (Fig. 3C). The band gap of the TiO_2 and $TiO_{2-x}N_x$ nanocrystals were calculated based on the absorption edge at ca. 385 nm. Their band gap was consistent with the intrinsic band gap absorption of pure anatase TiO_2 (3.2 eV) (a). In comparison to the bulk TiO_2, the $TiO_{2-x}N_x$ samples showed a distinct new absorption shoulder at around 390-530 nm after nitriding TiO_2 (b). This result merely indicates that nitrogen might be successfully incorporated into the lattice of TiO_2, which are anticipated to significantly alter the crystals and electronic properties of the self-doped $TiO_{2-x}N_x$ samples".

To inquire further proof for this indication, the presence of N atoms at the interstitial sites in $TiO_{2-x}N_x$ was also confirmed by a high resolution XPS of N1s with a binding energy of ca. 400.71 eV (Fig. 4). The XPS spectrum of N1s core electrons exhibits binding energies of 399.65, 400.57, 401.62 and 407.06 eV, respectively. The N1s peak at 399.65 and 400.57 eV were

attributed to the incorporated nitrogen in titania as interstitial N or O-Ti-N, while the N1s peak at 401.62 and 407.06 eV should be originated from the surface-adsorbed or contaminated nitrogen species.[20] Neither surface-adsorbed nor incorporated nitrogen was detected in the pristine TiO_2 nanocrystal (Fig. S8D).

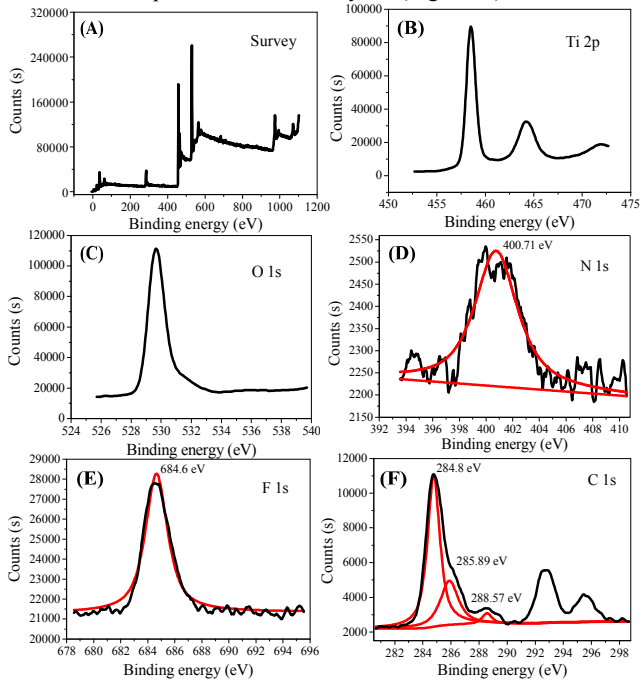

Fig. 4 XPS survey (A) and high-resolution spectra (B, C, D, E and F) for the $TiO_{2-x}N_x$ nanocrystals prepared by calcinating electrolyte in air at 500 ºC.

The XPS spectrum of F1s core electrons shows a binding energy at 684.6 eV (Fig. 4E), which is a typical value for fluorated TiO_2 systems and could be ascribed to F^- ions physically adsorbed on the TiO_2 surface (e.g., the surface Ti-F species formed by ligand exchange between F^- and surface hydroxyl groups, $\equiv Ti\text{-}OH + F^- \rightarrow \equiv Ti\text{-}F + OH^-$).[11] No signal for F^- in the lattice of TiO_2 (BE = 688.5 eV) was found. Thus, the atomic incorporation of F atoms or their substitution for O atoms in the anatase TiO_2 crystal lattice (doping) can be ruled out. Previous works have demonstrated that the formation of Ti-F bond can significantly lower the surface free energy of the {001} facets and reversely make them more stable than {101} facets, thus enabling the formation of anatase TiO_2 single crystals with a large percentage of reactive {001} facets.[20] However, it has been reported that the fluorinated surfaces of anatase TiO_2 single crystals can be easily treated to form clean, fluorine-free surface after heating at 600°C for a short time period (Fig. S8).[13]

The XPS spectra of C 1s showed several peaks at 284.65, 286.05 and ca. 288.5 eV (Figs. 4F and S8E). The C 1s peak at 284.65 eV is assigned to adventitious elemental carbon because of the residual carbon from the precursor solution and the hydrocarbon present in the XPS instrument itself, while the peaks at 286.05 and ca. 288.5 eV suggest the existence of carbonate species.[30] However, the peak around 281 eV, intrinsically resulting from the Ti-C bond, was not observed in the samples. Thus, all C was adsorbed onto the surface but not doped into the TiO_2 nanocrystals in our study.

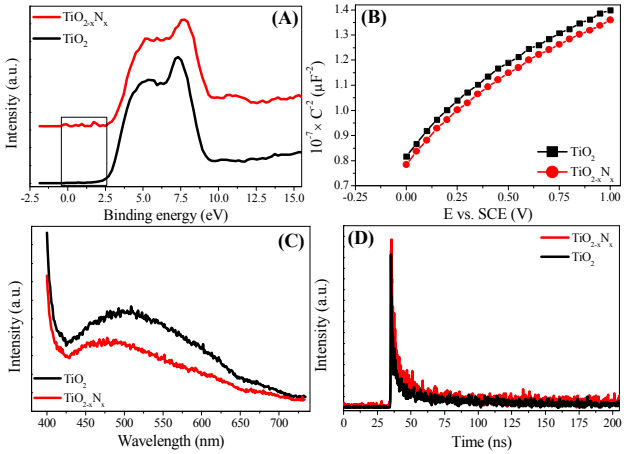

Fig. 5 VB XPS spectra (A), Mott-Schottky plots (B), steady fluorescence emission spectra (C) and time-resolved fluorescence decay spectra (D) of the TiO_2 and $TiO_{2-x}N_x$ nanocrystals.

The influence of N self-doping on the electric structure of TiO_2 nanocrystals was further investigated. As shown in Fig. 5A, the N self-doping by this method introduced new energy states mainly lie above the top of valence band of the TiO_2 nanocrystals, as illustrated in the indicative rectangle. Moreover, both the TiO_2 samples exhibited positive slopes as expected for n-type semiconductors, and a higher electron density was obtained in the $TiO_{2-x}N_x$ nanocrystals from the slopes of the Mott-Schottky plots (Fig. 5B).[31] From the above experimental results, it can be concluded that although the $TiO_{2-x}N_x$ crystals were not the direct band-gap semiconductor as validated by the measured DRS spectra in Fig. 3C, some significant modifications of their electric structures occurred during the self-doping process, which contributes to the visible light response and a higher electron density of the doped sample. Furthermore, the lower excitonic fluorescence emission intensity and its slower time-resolved decay kinetics indicate an enhanced separation and transfer as well as a prolonged lifetime of photocarriers in the $TiO_{2-x}N_x$ nanocrystals (Fig. 5C and D).[32] As a result, a superior photoactivity of the doped sample could be anticipated for practical applications.

3.3 Formation mechanism of the TiO_2 nanocrystals from the wasted ethylene glycol anodic electrolyte

The anodic formation of TNTs stratification layer in fluoric electrolytes occurred as a result of the interactions among the three simultaneous processes: the field-assisted oxidation (Reaction 1), the field-assisted dissolution (Reaction 2), and the chemical dissolution (Reaction 3).[1] The presence of fluorides strongly affects the anodization process to form water soluble $[TiF_6]^{2-}$ species through the field-assisted migration (Reaction 4).[1]

$$Ti + 2H_2O \rightarrow TiO_2 + 4H^+ + 4e^- \quad (1)$$

$$TiO_2 + 6F^- + 4H^+ \rightarrow [TiF6]^{2-} + 2H_2O \quad (2)$$

$$TiO_2 + 6HF \rightarrow [TiF6]^{2-} + 2H_2O + 2H^+ \quad (3)$$

$$Ti^{4+} + 6F^- \rightarrow [TiF_6]^{2-} \quad (4)$$

In this work, the $[TiF_6]^{2-}$ complex in the wasted electrolyte was utilized as both titanium and fluorin precursors for preparing {001}-exposed TiO_2 nanocrystals. Such a wasted anodic electrolyte was mainly comprised of newly-formed $(NH_4)_2TiF_6$

dissolved in the mixed organic-aqueous solvent with EG as a major component and water as a minor component, and its chemical compositions was a analyzed in details and the results are provided in Supporting Information (Figs. 1, S2 and S4). Furthermore, under acidic conditions fluoride ions could also accelerate crystallization and growth of TiO_2 due to a rapid in-situ "recrystallization", which would reduce the numbers of defects and impurities in the TiO_2 lattice (Reactions 5).[33]

$$[TiF_6]^{2-} + 2H_2O \rightarrow 4H^+ + TiO_2 + 6F^- \quad (5)$$

However, TiO_2 crystals prepared in water-based synthetic mediums (Reaction 5) usually exhibit irregular shapes and wide size distribution, due to the rapid nucleation and crystal growth. Comparatively, the alcoholysis route (Reactions 6 and 7) is superior for preparing nanomaterials with well-defined size and geometric shape, attributed to the smooth reaction and organic fluorides formation (R-F):[33]

$$\equiv Ti\text{-}F + R\text{-}OH \rightarrow \equiv Ti\text{-}OR + HF \quad (6)$$

$$Ti(OR)_n + TiF_n \rightarrow 2TiO_{n/2} + nRF \quad (7)$$

Moreover, some alcohols are able to promote the oriented crystal growth, and provide an effective means to design TiO_2 crystals with desired lattice planes as basal surfaces. For instance, 2-propanol can strengthen the stabilization effect associated with fluorine selective adsorption over {001} facets and thus stimulate its preferred crystal growth due to its multiple roles: 1) reaction medium; and 2) protecting agent to control the isotropic growth of anatase TiO_2 single crystals.[18] Likewise, in this work the residual EG electrolyte from anodic oxidation might be also adsorbed on the high-energy {001} facets. Consequently, the F species could be adsorbed and stabilized on the same facets to act as a synergistic capping agent and reaction medium together with usual HF. In this case, the subsequent calcination was indeed a "recrystallization".[13] As a result, high-quality anatase TiO_2 nanocrystals with a high percent of {001} facets could be synthesized. This morphology made the synthesis reaction thermodynamically favorable under acidic conditions in the presence of residual anodic electrolyte. EG tended to be heterolytically dissociated to form two alkoxy groups (-O-CH_2CH_2-O-) and subsequently bound to the coordinatively unsaturated Ti^{4+} cations on the (001) and (101) facets (Scheme 2). Moreover, the higher density of 5-fold Ti on (001) surfaces might lead to more significant selective adhesion of EG, and consequently change the adsorption energy of F over {001} to a more preferable state compared to {101}. This adsorption energy change would retard the growth of anatase TiO_2 single crystals along [001] direction.[6] Thus, the synergistic effects of coexistent chemisorbed alcohols and F could effectively retard the crystal growth along {001} direction, leading to the truncation of the octahedron with dominant {101} facets to the decahedron with dominant {001} facets.[18,34,35] As a consequence, the nanocrystals with dominant {001} facet could be obtained in this solvothermal alcoholysis route by calcinating the residual anodic electrolyte under appropriate conditions (Fig. 2).

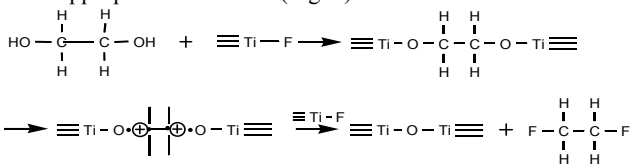

Scheme 2 Proposed possible mechanism for the alcoholysis of $[TiF_6]^{2-}$ to form TiO_2 nanocrystals by directly calcinating wasted anodic electrolyte.

Although the fresh electrolyte concentration, the anodic oxidation voltage and time as well as some other conditions might be key factors for this preparation process, it could be reasonably inferred that the wasted anodic electrolyte could be chemically resourced and the TiO_2 nanocrystals could be effectively prepared so long as sufficient $[TiF_6]^{2-}$ complex was produced. Moreover, considering the similar synergistic roles of alcohols in TiO_2 nanocrystals formation, this method might also be applied to other types of wasted anodic electrolyte with different alcohols. In addition, it should be also pointed out that some toxic gases, such as NH_3 and F_2, might simultaneously emit during the chemical recycle of wasted anodic electrolytes if they contain some toxic precursors, such as NH_4F. Therefore, gas collecting and adsorption systems should be installed.

3.4 Photochemical properties of the TiO_2 nanocrystals

Fig. 6A illustrates the current-voltage (*I-V*) characteristics of the annealed TiO_2 and $TiO_{2-x}N_x$ nanocrystals films on Ti metal photoelectrodes. The both *I-V* curves exhibited a typical characteristic asymmetric behavior. However, the contact electric resistance of the two photoelectrodes varied greatly with the direction of the applied external electric field, suggesting a strong intrinsic nanoscale effect.[36] Indeed, the observed intense rectifying behaviors of the TiO_2 semiconductor/metal junctions at the interface were intrinsically analogous to the *I-V* characteristics of n-type semiconductor/metal Schottky barrier diode. The measured responsive photocurrent intensity in Fig. 6B and C reflects the overall photoelectron-conversion process of the photocatalyst electrode. A higher photocurrent response usually means a lower electron-hole recombination and a higher photoelectron separation and transfer efficiency. These are beneficial for improving their photocatalytic activity and efficiency. Moreover, a visible light-driven photocurrent response and photoactivity of the $TiO_{2-x}N_x$ nanocrystals can be found in Fig. 6C. This further confirms the successful N self-doping under the appropriate calcination conditions as shown in Fig. 2B.

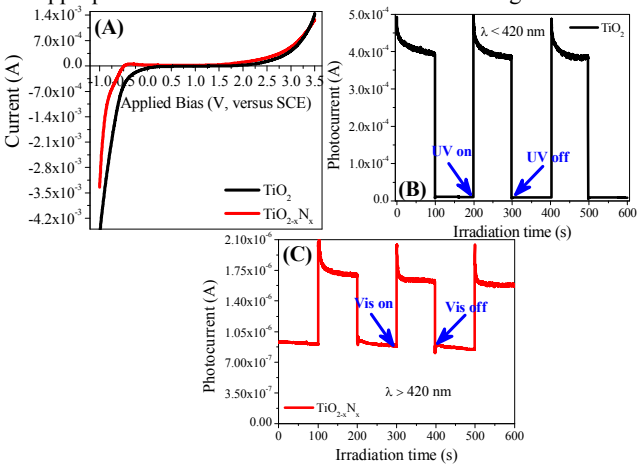

Fig. 6 *I-V* curves in dark (A) and short-circuit photocurrents (B and C) at + 0.30 V (versus SCE) of TiO_2 and $TiO_{2-x}N_x$ nanocrystals under UV and visible light irradiations respectively.

To evaluate the performance of these nanocrystals, their

photoactivities under both UV and visible light irradiations were examined by detecting the amount of generated •OH radicals.[37] The nanocrystals were suspended in terephthalic acid solution, and 200-420 (UV light) or 420-770 nm (visible light) with different irradiation times were applied. As shown in Fig. 7A and B, obvious fluorescence spectra associated with 2-hydroxy terephthalic acid were generated on the anatase TiO_2 and $TiO_{2-x}N_x$ nanocrystals upon irradiation. In contrast, no •OH radicals were detected on the non-doped anatase TiO_2 nanocrystals under visible light irradiation (Fig. 7C). A nearly linear relationship between fluorescence intensity and irradiation time was obtained (Fig. 7D), indicating the stability of the prepared TiO_2 and $TiO_{2-x}N_x$ nanocrystals.

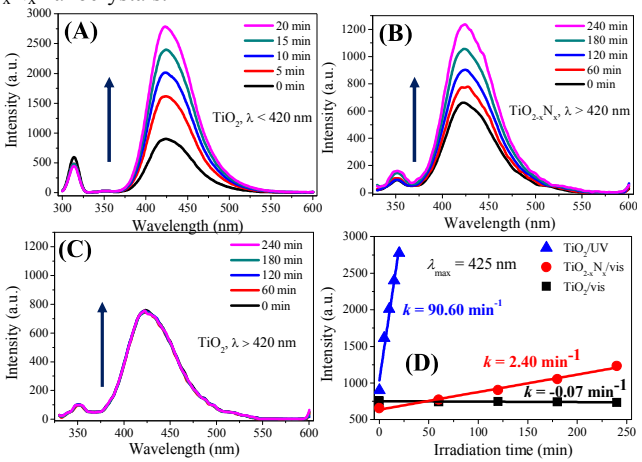

Fig. 7 Fluorescence spectra of UV irradiated TiO_2 (A), visible light irradiated $TiO_{2-x}N_x$ (B) and TiO_2 (C) suspensions in 3-mM terephthalic acid, respectively; (D) the linear relationship between the fluorescence intensity and the irradiation time.

These results clearly demonstrate a substantially enhanced photoactivity and photostability of the anatase TiO_2 nanocrystals with a large percentage of {001} facets. Such an enhancement could be attributed to the high density of unsaturated 5-fold Ti as well as their unique electronic structure. Furthermore, by regulating the calcination conditions, these anatase TiO_2 nanocrystals could be readily self-doped by N atom, so that their responsive spectra could be extended to visible light wavelength. These results agree well with the XRD, DRS and XPS measurements (Figs. 3 and 4).

3.5 Photodegradation of refractory pollutants by the prepared TiO_2 nanocrystals

Both the TiO_2 and $TiO_{2-x}N_x$ crystals exhibited a much higher photoactivity than the P25 benchmark for HAs and bentazone degradation (Fig. 8A). For HAs with an initial concentration of 10.75 mg/L TOC, nearly 100% removal was achieved with the TiO_2 crystals in 6 h, accompanied with a mineralization efficiency of 80% (Fig. S9). In contrast, only 70% HAs was removed with a low mineralization efficiency of 10% in 9 h under the identical conditions. These results clearly indicate that most of HAs were removed by the TiO_2 degradation, rather than by direct UV photolysis. Moreover, the TiO_2 crystals also showed a more than 2 times photoactivity as high as that of the P25 benchmark, as the observed pseudo-first-order HAs degradation rate constants were 0.389 and 0.142 h^{-1}, respectively (Fig. S10). Considering the low concentration of HAs in drinking water, a lower concentration (1.98 mg/L TOC) was effectively removed in 2 h (Fig. 8B), which was also much higher than that for P25.

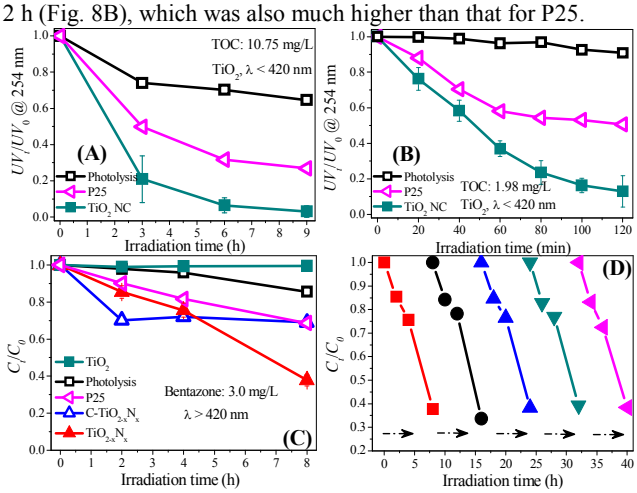

Fig. 8 Removal of HAs by TiO_2 crystals under UV (A,B) and bentazone by $TiO_{2-x}N_x$ crystals under visible light (C, D).

On the other hand, the yellow-color $TiO_{2-x}N_x$ crystals exhibited a relatively high visible light-driven photoactivity, and approximately 65% of 3 mg/L bentazone was removed in 8 h (λ>420 nm) (Fig. 8C), accompanied with a mineralization of nearly 35%. Comparatively, almost no removal was observed for both the photolysis and the white-color TiO_2. Approximately 30% of bentazone was removed by P25 due to the presence of 20% rutile phase, which is photoactive to visible light (Fig. S11). Moreover, the 5-run cyclic degradation tests further indicate the good stability of the $TiO_{2-x}N_x$ crystals (Fig. 8D). In addition, the gray-color C-$TiO_{2-x}N_x$ with a ca. C at.% of 19.16 calcinated at 400°C (Figs. 2, S4, S5 and S12) removed bentazone in the initial 2 h only (Figs. 8C and S11E), which was probably caused by physiochemical adsorption of the remained carbon (Fig. S13). Thus, to achieve a desirable N self-doping and visible-light-driven photoactivity of TiO_2 crystals, the calcination temperature should be ensured to be higher than 400°C, but lower than 550°C.

4. Conclusions

A facile and effective method was developed to prepare pristine and N-doped TiO_2 nanocrystals with exposed {001} facets by recycling wasted anodic electrolyte containing EG. Moreover, the prepared both pristine and N-doped TiO_2 nanocrystals are highly efficient for pollutant degradation. Compared with Degussa P25, one of the best commercial TiO_2 photocatalysts, the pristine nanocrystals showed a much higher degradation efficiency for humic acids under UV irradiation. The N-doped nanocrystals exhibited a nearly twice higher degradation efficiency for bentazone under visible light irradiation. Thus, the TiO_2 nanocrystals prepared by this method could be effectively used for photocatalytic water treatment.

Acknowledgements

The authors wish to thank the National Basic Research Program of China (2011CB933700), the National Science Foundation of China (51208488) and the Program for Changjiang Scholars and Innovative Research Team in University of the Ministry of Education of China for the partial support of this work.

Notes and references

[*] *Department of Chemistry, University of Science & Technology of China, Hefei, 230026, China. Fax: +86-551-63601592; E-mail: hqyu@ustc.edu.cn*

† Electronic Supplementary Information (ESI) available: Preparation of wasted anodic electrolyte, the influences of calcination conditions and electrolyte concentration on TiO_2 NCs growth, additional XPS and photocatalytic degradation datas. See DOI: 10.1039/b000000x/

1 P. Roy, S. Berger and P. Schmuki, *Angew. Chem. Int. Ed.* 2011, **50**, 2904-2939.

2 A. Y. Zhang, M. H. Zhou, L. Liu, W. Wang, Y. L. Jiao, Q. X. Zhou, *Electrochimica Acta* 2010, **55**, 5091-5099.

3 M. N. Chong, B. Jin, C. W. K. Chow and C. Saint, *Water Res.* 2010, **44**, 2997-3027.

4 M. D. Hernández-Alonso, F. Fresno, S. Suarez and J. M. Coronado, *Energy Environ. Sci.*, 2009, **2**, 1231-1257.

5 X. Quan, S. G. Yang, X. L. Ruan and H. M. Zhao, *Environ Sci Technol*, 2005, **39**, 3770-3775.

6 Y. W. Jun, M. F. Casula, J. H. Sim, S. Y. Kim, J. Cheon and A. P. Alivisatos, *J. Am. Chem. Soc.*, 2003, **125**, 15981-15985.

7 D. Q. Zhang, G. S. Li, X. F. Yang and J. C. Yu, *Chem. Commun.*, 2009, **29**, 4381-4383.

8 S. W. Liu, J. G. Yu and M. Jaroniec, *Chem. Mater.*, 2011, **23**, 4085-4093.

9 W. Q. Fang, X. Q. Gong and H. G. Yang, *J. Phys. Chem. Lett.*, 2011, **2**, 725-734.

10 G. Liu, J. C. Yu, G. Q. Lu and H. M. Cheng, *Chem. Commun.*, 2011, **47**, 6763-6783.

11 C. Z. Wen, H. B. Jiang, S. Z. Qiao, H. G. Yang and G. Q. Lu, *J. Mater. Chem.*, 2011, **21**, 7052-7061.

12 K. L. Ding, Z. J. Miao, Z. M. Liu, Z. F. Zhang, B. X. Han, G. M. An, S. D. Miao and Y. Xie, *J. Am. Chem. Soc.*, 2007, **129**, 6362-6363.

13 H. G. Yang, C. H. Sun, S. Z. Qiao, J. Zou, G. Liu, S. C. Smith, H. M. Cheng and G. Q. Lu, *Nature*, 2008, **453**, 638-641.

14 F. Amano, O. O. Prieto-Mahaney, Y. Terada, T. Yasumoto, T. Shibayama and B. Ohtani, *Chem. Mater.*, 2009, **21**, 2601-2603.

15 X. Han, Q. Kuang, M. Jin, Z. Xie and L. Zheng, *J. Am. Chem. Soc.*, 2009, **131**, 3152-3153.

16 H. B. Jiang, Q. Cuan, C. Z. Wen, J. Xing, D. Wu, X. Q. Gong, C. Z. Li and H. G. Yang, *Angew. Chem. Int. Ed.*, 2011, **50**, 3764-3768.

17 S. W. Liu, J. G. Yu and M. Jaroniec, *J. Am. Chem. Soc.*, 2010, **132**, 11914-11916.

18 H. G. Yang, G. Liu, S. Z. Qiao, C. H. Sun, Y. Jin, S. C. Smith, J. Zou, H. M. Cheng and G. Q. Lu, *J. Am. Chem. Soc.*, 2009, **131**, 4078-4083.

19 R. Asahi, T. Morikawa, T. Ohwaki, K. Aoki and Y. Taga, *Science*, 2001, **293**, 269-271.

20 G. Liu, H. G. Yang, X. W. Wang, L. N. Cheng, J. Pan, G. Q. Lu and H. M. Cheng, *J. Am. Chem. Soc.*, 2009, **131**, 12868-12869.

21 G. Liu, C. H. Sun, S. C. Smith, L. Z. Wang, G. Q. Lu and H.M. Cheng, *J. Colloid. Interf. Sci.*, 2010, **349**, 477-483.

22 W. Q. Luo, C. Y. Fu, R. F. Li, Y. S. Liu, H. M. Zhu and X. Y. Chen, *Small*, 2011, **7**, 3046-3056.

23 Q. J. Xiang, J. G. Yu, W. G. Wang and M. Jaroniec, *Chem. Commun.*, 2011, **47**, 6906-6908.

24 Q. J. Xiang, J. G. Yu and M. Jaroniec, *Phys. Chem. Chem. Phys.*, 2011, **13**, 4853-4861.

25 J. G. Yu, G. P. Dai, Q. J. Xiang and M. Jaroniec, *J. Mater. Chem.*, 2011, **21**, 1049-1057.

26 X. Zong, Z. Xing, H. Yu, Z. G. Chen, F. Q. Tang, J. Zou, G. Q. Lu and L. Z. Wang, *Chem. Commun.*, 2011, **47**, 11742-11744.

27 T. W. Woolerton, S. Sheard, E. Pierce, S. W. Ragsdale and F. A. Armstrong, *Energy Environ. Sci.*, 2011, **4**, 2393-2399.

28 W. R. McNamara, R. L. Milot, H. Song, R. C. Snoeberger III, V. S. Batista, C. A. Schmuttenmaer, G. W. Brudvig and R. H. Crabtree, *Energy Environ. Sci.*, 2010, **3**, 917-923.

29 M. Myahkostupov, M. Zamkov and F. N. Castellano, *Energy Environ. Sci.*, 2011, **4**, 998-1010.

30 X. X. Yang, C. D. Cao, K. Hohn, L. Erickson, R. Maghirang, D. Hamal and K. Klabunde, *J. Catal.*, 2007, **252**, 296-302.

31 J. J. Deng, X. X. Lv, J. Gao, A. W. Pu, M. Li, X. H. Sun and J. Zhong, *Energy Environ. Sci.*, 2013, **6**, 1965-1970.

32 M. Planells, L. Pellejà, J. N. Clifford, M. Pastore, F. D. Angelis, N. López, S. R. Marder and E. Palomares, *Energy Environ. Sci.*, 2011, **4**, 1820-1829.

33 X. Chen and S. S. Mao, *Chem. Rev.*, 2007, **107**, 2891-2959.

34 J. H. Liao, L. Y. Shi, S. Yuan, Y. Zhao and J. H. Fang, *J. Phys. Chem. C*, 2009, **113**, 18778-18783.

35 J. Zhu, S. H. Wang, Z. F. Bian, S. H. Xie, C. L. Cai, J. G. Wang, H. G. Yang and H. X. Li, *CrystEngComm*, 2010, **12**, 2219-2224.

36 A. Y. Zhang, M. H. Zhou, L. Han, Q. X. Zhou, *Appl. Catal. A.*, 2010, **385**, 114-122.

37 G. Liu, L. Z. Wang, C. H. Sun, X. X. Yan, X. W. Wang, Z. G. Chen, S. C. Smith, H. M. Cheng and G. Q. Lu, *Chem. Mater.*, 2009, **21**, 1266-1274.